Evidence for parallel junctions within high-T_c grain-boundary junctions

E. A. Early, R. L. Steiner, and A. F. Clark
National Institute of Standards and Technology, MET B-258, Gaithersburg, Maryland 20899

K. Char
Conductus, Inc., 969 West Maude Avenue, Sunnyvale, California 94086

(Received 15 September 1993; revised manuscript received 11 April 1994)

Half-integral constant voltage steps were observed in many high-T_c grain-boundary Josephson junctions of $YBa_2Cu_3O_{7-\delta}$ when a microwave field was applied. Five distinct observed behaviors of the widths of both integral and half-integral steps as a function of microwave amplitude, $\Delta I_{dc}(I_{ac})$, are reproduced by simulations of two or three junctions in parallel. This provides quantitative evidence that a single high-T_c grain-boundary junction is composed of several junctions in parallel. These junctions are formed by the overlap of superconducting filaments on either side of the grain boundary, and the spacing between ones with relatively large critical currents is $\sim 20\ \mu$m.

I. INTRODUCTION

We present experimental results on half-integral constant voltage steps in high-T_c grain-boundary junctions. Quantitative comparisons between these results and those obtained by simulations of parallel arrays of junctions enable us to draw conclusions about the microstructure of high-T_c grain-boundary junctions.

One common method for making Josephson junctions in high-T_c materials is to isolate individual grain boundaries.[1-3] There is accumulating evidence that these grain-boundary junctions are inhomogeneous on a microscopic scale. Early results on the magnetic-field dependence of the critical current of such junctions showed a complicated behavior,[1,4,5] and one particular behavior was well described by assuming a spatially nonuniform junction.[6] A residual critical current even at high magnetic fields[5-9] has been taken as evidence that a grain-boundary junction is composed of a parallel array of junctions. Measurements of $1/f$ noise are also well described by assuming that there are a number of parallel normal and superconducting connections across a grain boundary.[10,11] Finally, recent electromigration experiments indicate that superconductivity within the bulk film and across a grain boundary is filamentary.[12]

Recently, we observed unusual half-integral constant voltage steps in high-T_c $YBa_2Cu_3O_{7-\delta}$ grain-boundary junctions.[13] A typical current-voltage (I-V) curve for such a junction at 4.2 K irradiated with microwaves at a frequency $\nu \cong 9.3$ GHz is shown in Fig. 1. Note that the curve is symmetric about the origin. To understand this curve, first consider the usual ac Josephson effect.[14] Subjecting a junction to an ac field causes constant voltage steps, also called Shapiro steps,[15] to appear in the I-V curve. The voltages, V, of these steps are given by

$$V = n\nu/K_J ,$$

where n is the frequency of the ac field, $K_J = 2e/h = 0.483\,597\,9$ GHz/μV is the Josephson constant, and n is an integer. Thus, these steps are termed integral steps. For the case shown in Fig. 1, at $\nu \cong 9.3$ GHz integral steps occur at $V \simeq n \cdot 20\ \mu$V and are labeled accordingly for positive current polarity. The $n = 0$ step is along the current axis. In addition to these steps, there are distinct steps with voltages given by half-integral n, e.g., with $n = \frac{1}{2}, \frac{3}{2}, \frac{5}{2}$, etc. These are labeled for negative current polarity and are termed half-integral steps.

The concept of step width is important for understanding the results presented in this paper. The step width ΔI_{dc} is simply the range of dc current over which the voltage of a step is constant. Thus, for example, the step width of the $n = 2$ step shown in Fig. 1 is approximately 35 μA. The step width is a function of the applied microwave power, and at the microwave power at which the curve in Fig. 1 was obtained, the $n = \frac{5}{2}$ step is absent.

We have previously proposed that half-integral steps are a result of a single grain-boundary junction actually being composed of many junctions in parallel.[13] We present here more extensive experimental results of the

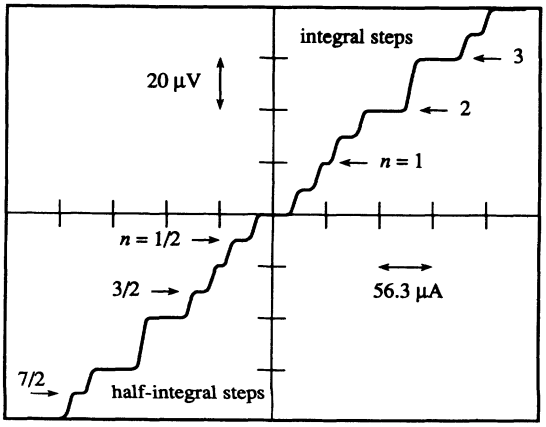

FIG. 1. Current-voltage curve of a 50-μm-wide junction at 4.2 K in a microwave field of 9.3 GHz. Both integral and half-integral steps are indicated by arrows and indexed by n.

magnetic-field dependence of the critical current and of the microwave amplitude dependence of step widths for many grain-boundary junctions. Comparisons of these experimental results with simulation results provide compelling evidence that there are multiple parallel junctions within a single high-T_c grain-boundary junction.

II. EXPERIMENTAL DETAILS

The grain-boundary junctions of $YBa_2Cu_3O_{7-\delta}$ were made using a biepitaxial process described previously.[16,17] The rotation angle at the grain boundary between the two films was 45°, the film thickness was about 0.25 μm, and the widths of the junctions varied between 5 and 50 μm. We measured 18 different junctions on seven chips from four different batch runs. For electrical measurements, copper wires were connected with indium to gold contact pads on each chip, which was then attached to a Styrofoam block with Teflon clips and placed in an X-band (6.5–13 GHz) rectangular waveguide. The chip was cooled in liquid nitrogen in an unshielded glass Dewar, and then cooled to its final temperature in liquid helium in a magnetically shielded metal Dewar. The majority of the measurements were performed at 4.2 K, and temperatures greater than this were measured with a Pt resistance thermometer.

A slowly varying (36 Hz) current was applied to a junction, and the resulting I-V curve was displayed on an oscilloscope. Microwaves of frequency close to 9.5 GHz were applied to the junction through the waveguide, and their power was measured at a coaxial T connector between the source and the waveguide. A magnetic field was applied to the junction either from a small solenoid placed beneath the chip or from a larger solenoid wrapped around the outside of the waveguide. The small solenoid had a maximum field less than 0.5 mT while the large solenoid was capable of achieving a field of 10 mT. The junction was approximately in the middle of the large solenoid. With no magnetic or microwave field, the normal-state resistance R_n of a junction was measured as the slope of the I-V curve at currents several times that of the critical current I_c. Since I_c is modulated by a magnetic field, the critical current of the junction was taken to be the maximum I_c obtained from varying the magnetic field. With a microwave field, the width of a step ΔI_{dc} was measured from the I-V curve displayed on the oscilloscope screen.

III. EXPERIMENTAL RESULTS

With no applied microwave or magnetic fields, the I-V curves of all junctions were similar to that for a weak-link junction described by the resistively-shunted-junction (RSJ) model.[18,19] There was a sharp onset of finite voltage at a definite critical current I_c, with no excess current at currents several times I_c and no hysteresis. Thus, these junctions are overdamped and the Stewart-McCumber parameter β_c is less than one.[18,19] In the following sections, experimental results describing general properties of the occurrence of half-integral steps, the dependence of the critical current on magnetic field, and the dependence of step widths on microwave power are presented.

A. Occurrence of half-integral steps

When half-integral steps were first noticed, no external magnetic field was applied and they occurred intermittently with cooldown history in the wider junctions (width ≥ 40 μm). Also, the critical currents of the junctions varied with cooldown history. In other words, a junction could have half-integral steps and a relatively small I_c after one cooldown and a relatively large I_c and no half-integral steps after a subsequent cooldown. Since the cooldown history of the junction was obviously important, we postulated that the amount of trapped magnetic field either in or near the junction was determining both the size of I_c and the occurrence of half-integral steps. It is reasonable to assume that magnetic field was trapped when the junction was cooled in liquid nitrogen since the Dewar was not magnetically shielded.

In order to test this conjecture, magnetic fields from a small solenoid were applied to junctions. The magnetic field not only modulated I_c, as discussed in the next section, but it also determined whether or not half-integral steps occurred. There were values of the field for which only integral steps were present in the I-V curve of a junction when a microwave field was applied, while changing to a different value of magnetic field resulted in both integral and half-integral steps. In this way, we could determine if half-integral steps occurred for a particular junction. In general, half-integral steps occurred

TABLE I. Widths, normal-state resistances R_n, and critical currents I_c for all measured junctions. A "Y" in the right-most column indicates that half-integral steps were observed for that junction.

Junction width (μm)	R_n (Ω)	I_c (μA)	Half-integral steps?
5	5.6	62	
10	2.8	76	
15	2.3	89	
20	0.97	37	
20	2.0	83	
20	1.2	140	
20	0.67	190	Y
30	0.89	110	
30	0.63	250	Y
30	0.71	260	Y
30	0.73	310	Y
40	0.45	290	Y
40	0.36	540	Y[a]
50	2.5	68	
50	0.71	220	Y
50	0.71	260	Y[a]
50	0.41	320	Y[a]
50	0.25	1010	Y[a]

[a]Also third-integral constant voltage steps.

at values of magnetic field for which I_c was a minimum. The result of these investigations at 4.2 K for all the junctions is summarized in Table I, which lists the junctions in order of increasing width and, for equal widths, increasing I_c. The normal-state resistance R_n of each junction is also listed, and a "Y" in the right-most column indicates that half-integral steps were observed for that junction. An asterisk indicates that third-integral steps ($n=\frac{1}{3}, \frac{2}{3}, \frac{4}{3}$, etc.) were also observed. Note that there is, in general, an inverse relation between I_c and R_n. Also, the critical current density I_c of these junctions is 10^3-10^4 A/cm^2, compared to the value of J_c in the film, 10^6-10^7 A/cm^2.[16] This table is discussed again in Sec. IV C and is presented here to indicate the large number of junctions for which half-integral steps were observed.

B. Magnetic-field dependence of the critical current

With no microwave field and at 4.2 K, the magnetic field H dependence of the critical current, $I_c(H)$, was measured by applying, with the large solenoid, a magnetic field perpendicular to the plane of the junction substrate. The critical current at each field value was taken as one-half the current range, over both negative and positive polarities, of the zero-voltage state in the I-V curve. In most junctions, particularly the wider ones, I_c was not symmetric about the origin. The measured magnitude of $I_c(H)$ for junctions of widths 10, 30, and 50 μm are shown in Fig. 2. Note that the magnetic-field scale is much smaller in Figs. 2(b) and 2(c) than it is in Fig. 2(a). The most obvious feature in Fig. 2 is that $I_c(H)$ is very complicated. There is certainly no Fraunhofer diffraction pattern, in contrast to what is expected from a single junction. In addition, a Fourier analysis of the curves shows that there is no fundamental period of $I_c(H)$. Qualitatively, it is apparent from Fig. 2 that the period decreases with increasing width of the junction, but it is ambiguous as to whether the period is proportional to the square of the width, as has been reported previously.[20] Also, the trend is for increasing I_c with increasing junction width, as can also be seen in Table I.

For the narrower junctions, those with widths ≤ 15 μm, there are values of the magnetic field for which I_c is zero, but I_c is always finite for the wider junctions. At low maximum fields (<0.5 mT) $I_c(H)$ is nonhysteretic with the direction of field sweep, but at a higher maximum field (10 mT) there is hysteresis. Also, I_c is never zero for the wider junctions even at the maximum field of 10 mT, in agreement with previous results.[7-9] With increasing temperature, the qualitative periodicity of I_c does not change, although the maximum I_c does decrease. To summarize, $I_c(H)$ is complicated, but in general the qualitative period of I_c decreases as the width of the junction increases.

C. Microwave amplitude dependence of step widths

Much information about half-integral steps was gained by measurements of step widths as a function of microwave power. With the junction at 4.2 K and microwave power constant, variations in the magnetic field produced values of I_c for which half-integral steps either were, or were not, observed in the I-V curve. Once an interesting value of I_c was found, the magnetic field was fixed and the widths of both integral and half-integral steps were measured at discrete values of microwave power. The microwave amplitude to which the junction is responding is proportional to the square root of the measured microwave power. The exact constant of proportionality is unknown, as it depends on the ratio of the measured power to the power in the waveguide and the coupling of the microwaves to the junction. The microwave amplitude is denoted by I_{ac} in order to illustrate its correspondence with the normalized ac current amplitude i_{ac} used in the simulations.

When only integral steps were present in the I-V curves, a plot of step width as a function of microwave amplitude, $\Delta I_{dc}(I_{ac})$, had behavior equivalent to that given by the RSJ model.[21] The maximum value of ΔI_{dc} alternated between the even and odd steps with increasing I_{ac}. When half-integral steps were also present in the I-V curves, however, a variety of behaviors were observed. These behaviors are classified into five different types, with representative experimental data from four different junctions illustrating these types shown in Fig. 3. Here, the step width ΔI_{dc} for integral and half-integral steps is plotted as a function of microwave ampli-

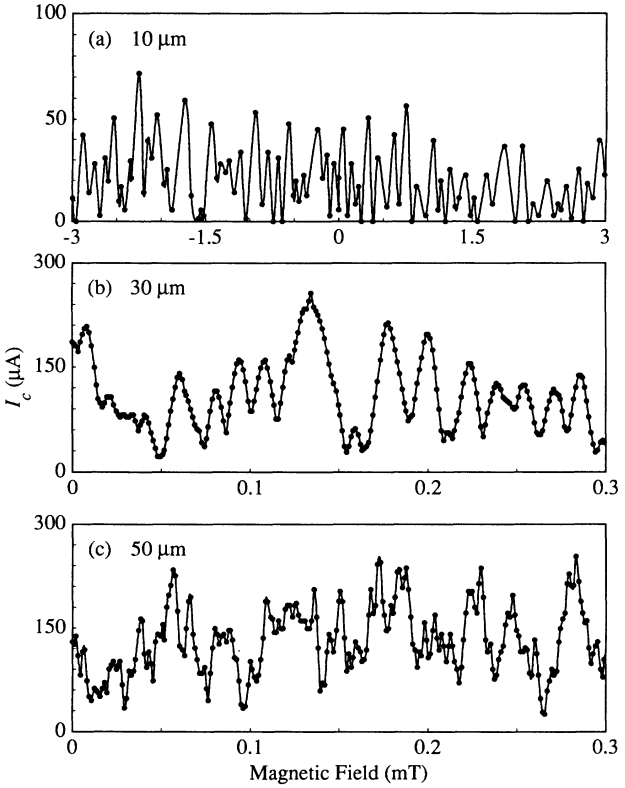

FIG. 2. Critical current I_c as a function of applied magnetic field at 4.2 K for junctions with widths (a) 10 μm, (b) 30 μm, and (c) 50 μm. The circles are data points, while lines are guides to the eye. Note that the horizontal scale of (a) is 20 times that of (b) and (c).

tude I_{ac}, which has been normalized to the maximum value for each set of data. The five types of behaviors for the integral and half-integral steps are shown in Figs. 3(a)–3(e), and for each figure the panels correspond, from top to bottom, to the $n=0, \frac{1}{2}, 1, \frac{3}{2}$, and 2 steps, as indicated in Fig. 3(a). Figure 3(f) shows $\Delta I_{dc}(I_{ac})$ for third-integral steps, which were not commonly observed, along with widths of integral and half-integral steps. The figures are arranged in approximately decreasing frequency of occurrence of the behaviors. Thus, the behavior shown in Fig. 3(a) was fairly common, while that shown in Fig. 3(e) was rare.

The five different behaviors are classified according to the individual behaviors of $\Delta I_{dc}(I_{ac})$ for the integral and half-integral steps. With half-integral steps present, the behavior of $\Delta I_{dc}(I_{ac})$ of the integral steps is never exactly like that given by the RSJ description of a single junction.[21] However, the behavior can be very similar, as shown in Fig. 3(e), which is termed RSJ behavior. There is a smooth, single-lobed variation of ΔI_{dc} between zero

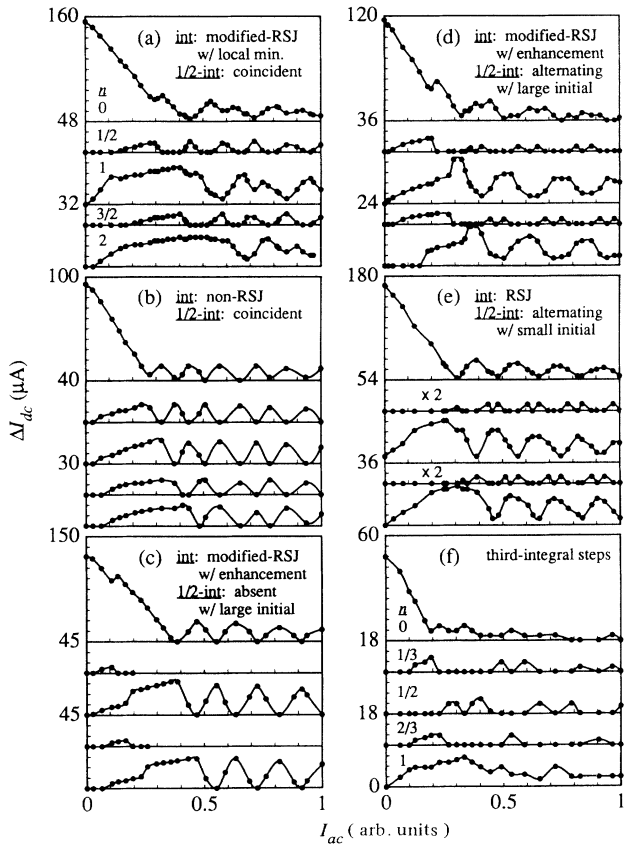

FIG. 3. Step width ΔI_{dc} as a function of microwave amplitude I_{ac} showing five different behaviors of the integral and half-integral step widths in (a)–(e) and the occurrence of third-integral steps in (f). The circles are data points and the lines are guides to the eye. In (a)–(e) the panels correspond, from top to bottom, to the $n=0$, $\frac{1}{2}$, 1, $\frac{3}{2}$, and 2 steps, as indicated in (a). The behaviors of the integral and half-integral step widths are classified in (a)–(e) by the descriptions following *int* and $\frac{1}{2}$-*int*, respectively, and are explained in the text. Although the units of I_{ac} are arbitrary, they are the same for each figure.

widths, and the maximum widths alternate between the even and odd steps with increasing I_{ac}, just as in the RSJ description. As for slight differences, maxima in ΔI_{dc} are not midway between minima and ΔI_{dc} for the $n=1$ and 2 steps is never zero at finite I_{ac}. With a *modified-RSJ* behavior of $\Delta I_{dc}(I_{ac})$ for the integral steps, there is still an alternation in the maximum widths between the even and odd steps, but now ΔI_{dc} does not vary smoothly between zero widths. Instead, the $n=0$ step has *local minima* in ΔI_{dc} that are in addition to the absolute minima present with RSJ behavior, as shown in Figs. 3(a), 3(c), and 3(d). For example, in Fig. 3(a) there are local minima in ΔI_{dc} for the $n=0$ step at $I_{ac}=0.3$, 0.6, and 0.85. For the $n=1$ and 2 steps, ΔI_{dc} can also have local minima, as in Fig. 3(a), or it can be *enhanced* at certain values of I_{ac}, as in Figs. 3(c) and 3(d). Specifically, in Fig. 3(c) there is an abrupt increase in ΔI_{dc} at $I_{ac}\approx 0.2$ for both the $n=1$ and 2 steps, while in Fig. 3(d) the increase occurs at $I_{ac}\approx 0.3$. Therefore, modified-RSJ behavior of $\Delta I_{dc}(I_{ac})$ for the integral steps is characterized either by local minima for all the integral steps or by local minima only for the $n=0$ step and enhancement for the $n=1$ and 2 steps. With *non-RSJ* behavior, shown in Fig. 3(b), there is again a smooth variation of ΔI_{dc} between zero widths for all integral steps. However, now the values of I_{ac} of maxima and minima of ΔI_{dc} are the same for all integral steps. In other words, whereas with RSJ behavior the maxima of ΔI_{dc} alternated between the even and odd steps with increasing I_{ac}, with non-RSJ behavior the maxima of ΔI_{dc} coincide with each other for all integral steps.

There are three types of behavior for $\Delta I_{dc}(I_{ac})$ of the half-integral steps. With coincident behavior, shown in Figs. 3(a) and 3(b), the maxima in ΔI_{dc} for both the $n=\frac{1}{2}$ and $\frac{3}{2}$ steps occur at the same values of I_{ac}. Another behavior is that for which half-integral steps are *absent* at all but the smallest microwave amplitudes, as shown in Fig. 3(c). With increasing I_{ac} half-integral steps are initially present, but they disappear after the first zero of ΔI_{dc}. This behavior is accompanied by a local minimum in ΔI_{dc} for the $n=0$ step and enhancement of ΔI_{dc} for the $n=1$ and 2 steps, followed by RSJ behavior of the integral steps for greater microwave amplitudes. The third distinct behavior of the half-integral step widths is shown in Figs. 3(d) and 3(e). Here, $\Delta I_{dc}(I_{ac})$ has a *paired and alternating* behavior in which, with increasing I_{ac}, there are two maxima in ΔI_{dc} for the $n=\frac{1}{2}$ step, followed by two maxima for the $n=\frac{3}{2}$ step, etc. This behavior can be subclassified into ΔI_{dc} for the half-integral steps at the smallest values of I_{ac} being *large*, as in Fig. 3(d), or *small*, as in Fig. 3(e). Similar to the behavior shown in Fig. 3(c), an initially large value of ΔI_{dc} for half-integral steps is accompanied by modified-RSJ behavior of the integral step widths with enhancements in ΔI_{dc} for the $n=1$ and 2 steps.

To summarize, the behavior of $\Delta I_{dc}(I_{ac})$ for integral steps is classified as RSJ, non-RSJ, or modified-RSJ with either local minima in or enhancement of ΔI_{dc} for the $n=1$ and 2 steps. For half-integral steps, the behavior is classified as either coincident, initially present and then

absent, or paired and alternating with initially small or large values of ΔI_{dc}. The appropriate classifications of the behavior of $\Delta I_{dc}(I_{ac})$ for the integral and half-integral steps are indicated in Fig. 3.

As for third-integral steps, shown in Fig. 3(f), it is difficult to ascribe a definite behavior to $\Delta I_{dc}(I_{ac})$ for the integral steps. In contrast, $\Delta I_{dc}(I_{ac})$ for the fractional steps does have a definite pattern. There is a repeating pattern of two maxima in ΔI_{dc} for the $n=\frac{1}{2}$ step, followed by maxima for the $n=\frac{1}{3}$, $\frac{2}{3}$, and $\frac{1}{3}$ steps in order. We have also observed third-integral steps in I-V curves in which no half-integral steps were present, and maxima in ΔI_{dc} of the $n=\frac{1}{3}$ and $\frac{2}{3}$ steps alternated with increasing I_{ac}.

A statement was made in the previous section on the occurrence of half-integral steps that, in general, half-integral steps occurred at minima in $I_c(H)$. A more quantitative experiment to test this statement was performed on a 40-μm-wide junction at 4.2 K, in which the critical current values and the occurrence of half-integral steps were recorded as a function of applied magnetic field, as shown in Fig. 4. For these measurements, the magnetic field was produced by the small solenoid, so the value of the field at the junction was unknown. The data for $I_c(H)$ are indicated by solid circles in Fig. 4, and the line is a guide to the eye. If the circle is not enclosed by another symbol, then there were no half-integral steps in I-V curves at that magnetic field and $\Delta I_{dc}(I_{ac})$ for the integral steps had RSJ behavior. A solid circle enclosed by another open symbol indicates that half-integral steps were observed in I-V curves, and the behavior of $\Delta I_{dc}(I_{ac})$ for the integral and half-integral steps was similar to that shown either in Fig. 3(a) or 3(d). Similar to Fig. 2, the $I_c(H)$ data shown in Fig. 4 is fairly complicated and not obviously periodic. It is also apparent that the occurrence of half-integral steps is correlated with minima in I_c, and not with absolute values of I_c. Half-integral steps were present in I-V curves at all the relative minima of $I_c(H)$ shown in Fig. 4 save one. However, for a constant value of I_c, such as $\sim$45 and $\sim$120 μA, half-integral steps occur only when $I_c(H)$ is a minimum.

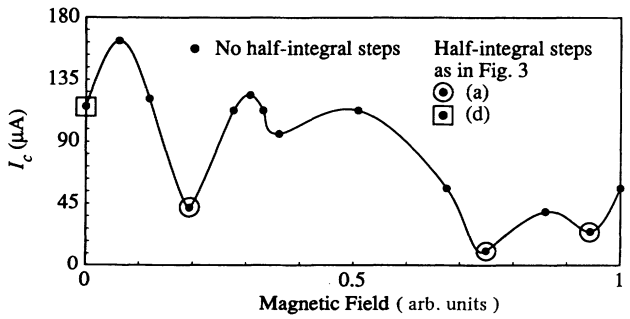

FIG. 4. Critical current I_c as a function of applied magnetic field for a 40-μm-wide junction at 4.2 K. Data points are solid circles, and a larger open enclosing symbol indicates the occurrence of half-integral steps with behavior similar to that shown in Fig. 3(a) for the circle or Fig. 3(d) for the square.

IV. DISCUSSION

In the original report of our observation of half-integral steps, we proposed that they were caused by a parallel array of junctions within a single grain-boundary junction.[13] We developed a model of a parallel array of Josephson junctions using the RSJ model for junctions without capacitance and including the effects of inductance, magnetic fields, and junction parameters. Here, we present selected simulation results of the dependence of the normalized step width on normalized ac current amplitude, $\Delta i_{dc}(i_{ac})$, that reproduce the experimental results shown in Figs. 3(a)–3(e).

Other possible causes for half-integral steps were considered and rejected in our previous paper, and we briefly summarize the arguments here. Half-integral steps are not caused by a subharmonic of the primary microwave frequency because the cutoff frequency of the X-band waveguide, 6.55 GHz, is greater than half the microwave frequency. A nonsinusoidal current-phase relation can cause fractional steps in single Josephson junctions,[22,23] but simulations[24–26] of $\Delta i_{dc}(i_{ac})$ do not reproduce the experimental behaviors shown in Fig. 3. Two-dimensional arrays have attracted considerable interest recently, and both giant and fractional Shapiro steps have been observed for current flowing in the plane of the array and a magnetic field applied perpendicular to this plane.[27,28] We, however, observed no giant Shapiro steps and the plane of a two-dimensional array in a grain-boundary junction would be perpendicular to the direction of current flow. Note that with this orientation a two-dimensional array is equivalent to a parallel array of junctions. Long junctions are considered in the next section.

A. Model of parallel junctions

Our model considers an array of N Josephson junctions in parallel, indexed by $j=0$ to $N-1$, each with a phase difference δ_j across it. The entire array has a critical current I_c and normal-state resistance R_n and is subjected to a current $I=I_{dc}+I_{ac}\sin(\omega t)$. This is an extension of previous models which considered only two junctions in parallel.[29–31] The primary assumption in our model is that the junctions are described by the RSJ model with no noise term, since nearly all experiments were performed at the temperature of liquid helium, and with no capacitance, since hysteresis was not observed in the experimental I-V curves. A further assumption is that the areas of the junctions perpendicular to the applied magnetic field are much smaller than the areas of the loops formed by adjacent junctions, so that the magnetic field affects only the phase differences of the junctions and not their maximum critical currents. In other words, single-junction magnetic effects are neglected. Finally, the areas of the loops are taken to be equal, so the inductances of the loops are also equal.

There are several important parameters in this model. The normalized frequency $\Omega=\nu/\nu_0$, where ν is the frequency of the applied microwaves and $\nu_0=(2e/h)I_cR_n$ is the characteristic frequency of a junction. The junction

critical currents $I_{c;j}$ can be unequal, described by $I_{c;j}=\eta_j I_c$ where the parameter η_j is the fraction of the array critical current carried by junction j. However, for all junctions $I_{c;j}R_j=I_cR_n$. The inductance L of the loops results in a dimensionless parameter $\beta_L=2\pi LI_c/\Phi_0$, where Φ_0 is the magnetic flux quanta. The magnetic field within the loops is divided into a normalized applied flux $f_a=\Phi_a/\Phi_0$ that is uniform across the array and a normalized trapped flux $f_{t;j}$ within each loop.

Simulation results were obtained by numerically solving the equations that describe the above model using the fourth-order Runge-Kutta method with a step size of $0.01(2\pi\nu_0 t)$. Plots of $\Delta i_{\rm dc}(i_{\rm ac})$ for fixed N, Ω, β_L, η_j, f_a, and $f_{t;j}$ were generated by finding the limits of $i_{\rm dc}$ for which $\phi_0=\sum_j\eta_j\delta_j$ advances by an average of $2\pi n$ in two ac cycles for a fixed value of $i_{\rm ac}$, following a previous suggestion by Belykh, Pedersen, and Soerensen[32] and implementation by Kautz.[33] The width of step n at that value of $i_{\rm ac}$ is then the difference between the minimum and maximum values of $i_{\rm dc}$, and this procedure is repeated for different values of n and $i_{\rm ac}$. The same technique was used for the dependence of the normalized critical current on normalized magnetic field, $i_c(f_a)$, for which $n=0$, $i_{\rm ac}=0$, and f_a is varied.

For the simulation results, $\Omega=0.175$ was chosen as representative of the experimental values. Using the values in Table I and $\nu=9.5$ GHz, Ω ranges from 0.057 to 0.201, except for one junction with $\Omega=0.547$. Also, the simulation results were not sensitively dependent on the value of Ω. For two junctions in parallel, $N=2$, there is no trapped flux since there is only one loop, $\eta_0=0.5$ means the junctions were equal, and $\beta_L=10$ yields good agreement with experimental results and is a reasonable value. For $N=3$, all the junctions are equal, the difference in trapped flux between the loops is $\Delta f_t=f_{t;1}-f_{t;2}$ (where $f_{t;2}=-f_{t;1}$ for symmetry), and $\beta_L=15$ for consistency with the results for $N=2$ since $\beta_L\propto I_c\propto N$.

B. Comparison of experimental and simulation results

For ease of comparison, the experimental results of $\Delta I_{\rm dc}(I_{\rm ac})$ from Figs. 3(a) to 3(e) are reproduced in Figs. 5(a)–5(e). To the right of each of these figures are selected simulation results of $\Delta i_{\rm dc}(i_{\rm ac})$, Figs. 5(f)–5(j). As usual, the panels in each figure correspond, from top to bottom, to the $n=0,\frac{1}{2},1,\frac{3}{2}$, and 2 steps. For the simulation results, the relevant parameters are given in each figure. Note the excellent agreement between experimental and simulation results in all cases shown in Fig. 5. All the behaviors of $\Delta I_{\rm dc}(I_{\rm ac})$ for both integral and half-integral steps described and classified in Fig. 3 are reproduced by the simulation results. In addition, there is agreement in nearly all of the finer details of integral step width as a function of ac current amplitude between experiments and simulations. Specifically, experimentally observed nonzero minima of $\Delta I_{\rm dc}$, asymmetric shapes of $\Delta I_{\rm dc}(I_{\rm ac})$, and even a slight decrease in $\Delta I_{\rm dc}$ for the $n=1$ step near

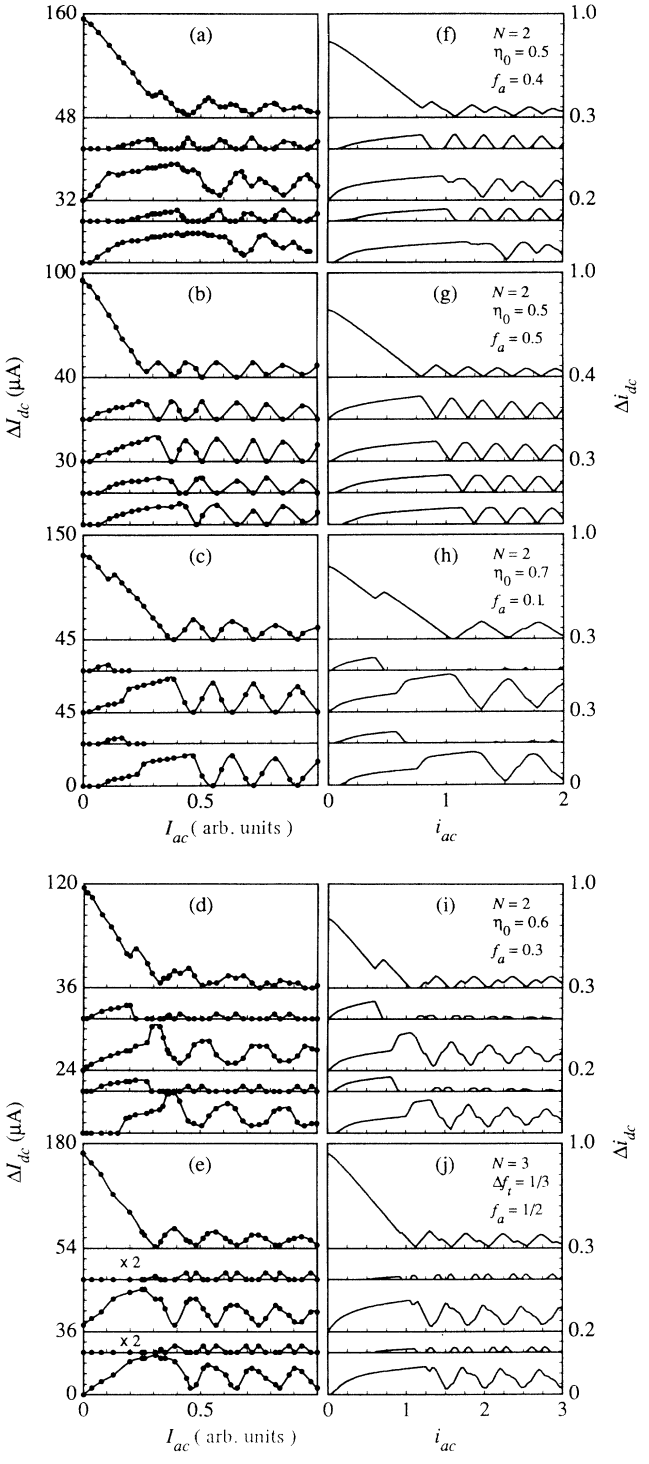

FIG. 5. (a)–(e) Experimental step width $\Delta I_{\rm dc}$ as a function of microwave amplitude $I_{\rm ac}$, reproduced from Fig. 3. (f)–(j) Simulation step width $\Delta i_{\rm dc}$ as function of ac current amplitude $i_{\rm ac}$ that reproduces the experimental result shown to the left of the figure. For the simulations, the number of junctions N, the applied magnetic flux f_a, the fraction of array critical current carried by the first junction η_0 for $N=2$, and the difference in trapped magnetic flux between the loops Δf_t for $N=3$ are indicated. For all simulations $\Omega=0.175$ and $\beta_L=10$ for $N=2$ and 15 for $N=3$. In all figures the panels correspond, from top to bottom, to the $n=0,\frac{1}{2},1,\frac{3}{2}$, and 2 steps.

its first maximum are reproduced in the simulation results. As shown in Fig. 4, half-integral steps occur experimentally at minima of $I_c(H)$. Likewise, the simulation results for $N=2$ shown in Fig. 5 are either close to or at minima of $i_c(f_a)$, Fig. 5(f) and Figs. 5(g)–5(i), respectively. Note too that β_L is essentially the only adjustable parameter in the simulations.

A few simulations of $\Delta i_{dc}(i_{ac})$ for third-integral steps were performed for $N=3$ with the parameters given above. They did not reproduce the behavior shown in Figs 3(f), although with no trapped flux and $f_a=\frac{1}{3}$ there were no half-integral steps and the maximum Δi_{dc} of the $n=\frac{1}{3}$ and $\frac{2}{3}$ steps alternated with increasing i_{ac}, which is similar to a behavior we have observed.

C. Model of grain-boundary junctions

The excellent agreement between experimental and simulation results shown in Fig. 5 is truly remarkable, especially considering that only two or three junctions in parallel are needed. This agreement is direct, quantitative evidence that high-T_c grain-boundary Josephson junctions are actually composed of a parallel array of junctions. It also allows us to propose a microstructural model of grain-boundary junctions.

1. Superconducting filaments

One possible explanation for the ability to reproduce the experimental results with only two junctions in parallel is that grain-boundary junctions could be considered as long. The criteria for a long junction, as opposed to a small one, is that the width of the junction be greater than twice the Josephson penetration depth $\lambda_J=\sqrt{\hbar/2e\mu_0 dJ_c}$.[14] Here, $d=2\lambda_L$, the critical current density of the junction is J_c, and λ_L is the London penetration depth of the superconductor, which is ≈ 170 nm along the a-b plane of $YBa_2Cu_3O_{7-\delta}$ at 4.2 K.[20] Using the widths and critical currents listed in Table I, λ_J for all the grain-boundary junctions is on the order of 5 μm. Therefore, all junctions wider than 10 μm could be considered as long. Also, no distinguishing features of long junctions are expected in the I-V curves of the grain-boundary junctions since overdamped long junctions have I-V curves that are similar to those of small junctions.[34] With a long junction and an applied magnetic field, the current through the junction is confined to the edges, resulting in two parallel junctions. If this is occurring in these grain-boundary junctions, then all junctions with widths greater than 10 μm should have half-integral steps. However, this is not in agreement with the experimental results shown in Table I, in which all but one of the 20-μm-wide junctions, and even one 50-μm-wide junction, do not have half-integral steps. Also, third-integral steps for $\Omega=0.175$ result from three junctions in parallel, which implies that in the wider junctions there are more than two junctions in parallel. Thus, these grain-boundary junctions should not be considered as long junctions.

There is an apparent contradiction between the results presented in Fig. 2 and those in Fig. 5. The very complicated and nonperiodic behavior of $I_c(H)$ implies that there are many junctions in parallel, as suggested by other authors.[5–9] However, the excellent agreement between the experimental and simulation behaviors of $\Delta I_{dc}(I_{ac})$ implies that there are only two, or at most three, junctions in parallel. The resolution of this apparent contradiction is provided by applying the model of Moeckly, Lathrop, and Buhrman for grain-boundary junctions.[12] In this model, superconductivity in the film is confined to randomly distributed filaments, with transverse dimensions between 1 and 60 nm, that terminate on either side of the grain boundary. Because the transverse dimensions of these filaments are less than the thickness of the film, ~ 250 nm, the ends of the filaments are randomly distributed in the plane of the grain boundary. Overlap of these ends on either side of the grain boundary forms small, weak-link Josephson junctions, with the critical current of each junction being proportional to the area of overlap. Because the distribution of ends in the plane is random, there is a smooth distribution of overlap areas and thus of junction critical currents. This microstructural model for grain-boundary junctions is shown schematically in Fig. 6 for a slice through the grain boundary and parallel to the plane of the substrate. The hatched areas are normal material, with the direction of the a-b plane indicated on either side of the grain boundary by both the axes and the hatching direction. The superconducting filaments are the clear areas (size exaggerated relative to the normal areas), all with approximately the same size but randomly distributed along both sides of the grain boundary. Thus, as illustrated in Fig. 6, there are some regions along the grain boundary where the overlap of two filaments is small, and other regions where the overlap is large. Consequently, there are many junctions within a grain-boundary junction, a few of which have large critical currents because of large overlap areas. This resolves the apparent contradiction posed above. Many junctions in parallel cause a very complicated behavior of $I_c(H)$, but only a few junctions have large critical currents, and these are the ones that determine the behavior of $\Delta I_{dc}(I_{ac})$ and make it possible to

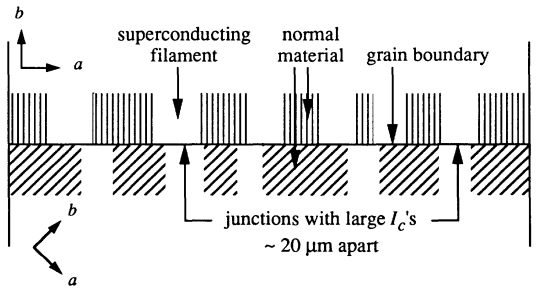

FIG. 6. Schematic representation of a cross section of the microstructure of a grain-boundary junction. Normal material is indicated by hatching, with the alignment of the a-b planes indicated by both the axes and the hatching direction, while the superconducting filaments are the clear areas (exaggerated size). A junction is formed by the overlap of two filaments on either side of the grain boundary. Junctions formed by large overlaps, and thus with large critical currents, are $\sim$20-μm apart, as discussed in the text.

reproduce this behavior by simulations with only two or three junctions in parallel.

Other consequences of this model are supported by the experimental results. The overlap of filaments across the grain boundary results in weak-link junctions with small capacitances. Such junctions are overdamped, in agreement with nonhysteretic experimental I-V curves, and further justifies ignoring capacitance in the simulations. The reduction of J_c in the grain-boundary junctions by a factor of 10^3 from its value in the film is consistent with this model. Some of the reduction is due to the depression of the superconducting order parameter at the junction,[35] while the remainder is caused by the failure of many filaments to overlap across the grain boundary. A slight slope of the steps is likely a result of a resistance in parallel with the junctions caused by the overlap of normal areas. Finally, the increase of I_c with junction width instead of its saturation as reported by Mayer *et al.*[36] is explained by this model. The number of junctions increases with the width of the grain-boundary junction, and thus I_c also increases with increasing width. There is no saturation because the dimensions of all the parallel junctions are small compared to λ_J.

2. *Separation between strong junctions*

Parallel junctions with relatively large critical currents, here called strong junctions, are indicated to be ~ 20 μm apart in Fig. 6. This separation distance is based upon the results presented in Table I, where the occurrence of half-integral steps is obviously correlated with the width of the grain-boundary junction. On average, those junctions with widths of 20 μm or less do not have half-integral steps, while those junctions of greater width do. A 20-μm separation between strong junctions accounts for this correlation. There are, of course, deviations from this because of the random distribution of junctions within a grain boundary. Thus, one 20-μm-wide junction has half-integral steps while one 50-μm-wide junction does not. There is also a correlation between the critical current of a junction and the occurrence of half-integral steps, with a cutoff of about 170 μA. Assuming two strong junctions, each with an I_c of 80 μA, and a bulk J_c of 10^7 A/cm^2, the transverse dimension of each junction is ~ 300 Å. This is consistent with dimensions of 10–600 Å deduced from $I_c(H)$ measurements[8] and from the filamentary model.[12]

Further support for the estimate of 20 μm between strong junction is again provided by Table I. Third-integral steps are present only in the wider grain-boundary junctions. Assuming that three strong junctions in parallel are necessary for third-integral steps, then on average only the 50-μm-wide junctions are wide enough to contain three strong junctions. Again, because of the randomness involved with the junctions, one 40-μm-wide junction has third-integral steps while two 50-μm-wide junctions do not. Also, the separation between strong junctions can be estimated from the value of β_L used in the simulations. Within a factor of 2, $\beta_L = 10$ for $N = 2$ resulted in the best agreement between experimental and simulation results. The inductance of a square hole in a superconducting film is $L = (5/4)\mu_0 W$, where W is the width of the hole.[37] For a typical $I_c = 250$ μA from Table I, the spacing between strong junctions is about 8 μm, which agrees well with the estimate of 20 μm from above considering the approximations used in arriving at this value. This agreement, together with the data in Table I, shows that on average the spacing between strong junctions within a grain boundary is 20 μm. Of course, this estimate is only for grain boundaries with a 45° rotation angle. The spacing could be different for grain boundaries with different rotation angles.

The microstructural model of a single grain-boundary junction being composed of many junctions in parallel, two or three of which have high critical currents, is further supported by simulations of six junctions in parallel. For these simulations, $\Omega = 0.175$, $\beta_L = 30$, and 80% of the array critical current was carried by two equal strong junctions separated by one of the four other equal junctions that carried the remainder. The results are shown in Fig. 7, where the array critical current is plotted as a function of applied field in Fig. 7(a), and the step widths are plotted as a function of ac current amplitude in Figs.

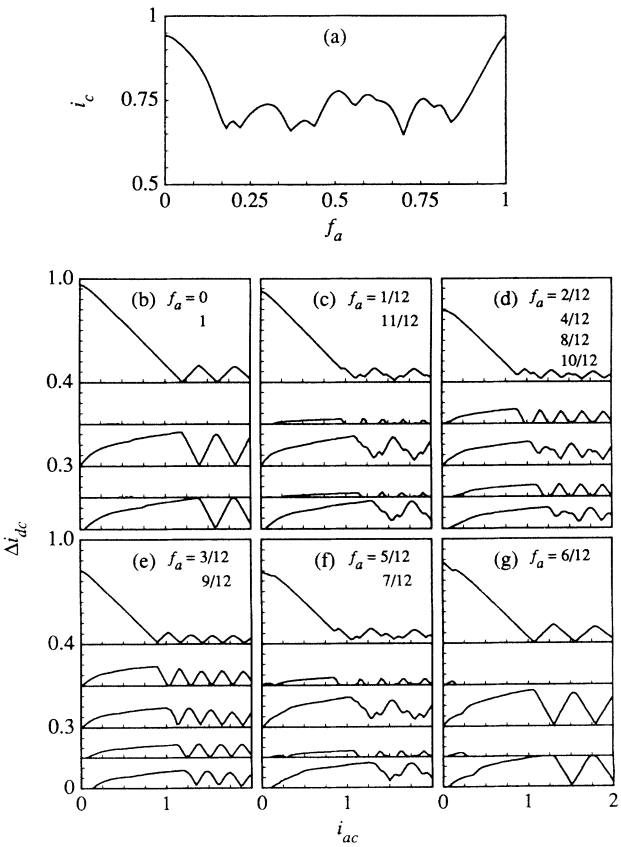

FIG. 7. Simulation results for $N = 6, \Omega = 0.175, \beta_L = 30$, with no trapped flux and with 80% of the array critical current carried by two junctions separated by one of the four equal junctions that carry the remainder of the critical current. (a) Array critical current i_c as a function of applied magnetic flux f_a. (b)–(g) Step width Δi_{dc} as a function of ac current amplitude i_{ac} at the indicated values of f_a. The panels in each figure correspond, from top to bottom, to the $n = 0, \frac{1}{2}, 1, \frac{3}{2}$, and 2 steps.

7(b)–7(g) at the indicated values of applied flux. The behavior of $i_c(f_a)$ in Fig. 7(a) is complicated with no obvious regular periodicity between $f_a=0$ and 1, although it is periodic in one flux quanta. This periodicity is present because the parallel array model assumes that the areas of the individual junctions are much less than the areas of the loops formed by the junctions. Thus, there is no Fraunhofer diffraction envelope in $i_c(f_a)$. In actual grain-boundary junctions, though, there are numerous parallel junctions of various finite sizes, each contributing a Fraunhofer envelope. This further complicates $I_c(H)$ and makes direct comparison with simulations of $i_c(f_a)$ difficult. There is also no symmetry in $i_c(f_a)$ about $f_a=\frac{1}{2}$, although the behavior of $\Delta i_{dc}(i_{ac})$ is symmetric about $f_a=\frac{1}{2}$, as shown in Figs. 7(b)–7(g). These behaviors are similar to those for only two junctions in parallel. Specifically, compare Figs. 7(d) and 5(f), Figs. 7(e) and 5(g), and Figs. 7(g) and 5(h). The behavior shown in Fig. 7(e) is particularly noteworthy. With only two junctions, this behavior is obtained for $f_a=\frac{1}{2}$. With six junctions, this same behavior is obtained with $f_a=\frac{1}{4}$, which corresponds to half a flux quanta between the two strong junctions. Therefore, these two junctions dominate the behavior of $\Delta i_{dc}(i_{ac})$ for six junctions in parallel, making it nearly equivalent to that of only two junctions.

3. *Distribution of parallel junctions*

Despite the excellent agreement between experimental and simulation results, actual grain-boundary junctions are likely to be more complicated than the above model suggests. Trapped flux, which depends on the cooldown history of the junction, could change the apparent number of strong junctions in parallel. As an example, the behaviors of $\Delta I_{dc}(I_{ac})$ shown in Figs. 5(a) and 5(e) were obtained with the same junction but after different cooldowns, and are reproduced with two and three junctions in parallel, respectively. There are also indications that the distribution of critical currents of the parallel junctions within a grain boundary are not random. Assuming a random distribution of equally sized superconducting filaments on each side of the grain boundary, there is an exponential decrease in a histogram of the number of junctions as a function of critical current. Simulations of 16 junctions in parallel with this distribution of critical currents have a noisy behavior of $\Delta i_{dc}(i_{ac})$ with no correspondence to the behavior of only two junctions in parallel. For the simulations of six junctions in parallel discussed above, the behavior of $\Delta i_{dc}(i_{ac})$ is like that for two junctions in parallel only if the two strong junctions carry over 70% of the critical current of the array.

Consequently, it seems likely that there are preferred relative critical currents of the parallel junctions. In other words, instead of a monotonic distribution of the number of junctions as a function of critical current, there is a bimodal distribution with many junctions having relatively small critical currents and only a few having much larger critical currents. One possible mechanism is that there are different types of parallel junctions. If the superconducting filaments occupy a small fraction of the area on each side of the grain boundary, then only a few filaments will overlap across the grain boundary. The few junctions formed in this way could have a much greater critical current than those formed between filaments that were close to each other but did not overlap. Another possibility is that there is some ordering of the filaments within the film. Then, structural models of grain-boundary junctions[38] may be important, as the structure of the grain boundary could favor certain overlap areas of the filaments on either side.

A related consideration is the reproducibility of grain-boundary junctions. The random distribution of filaments assumed in the model presented above implies that junction parameters will have some variability. This is indeed the case experimentally, as shown in Table I, in which different junctions with the same widths have a wide range of parameters. As described in the previous paragraph, there could be some ordering of the filaments at the grain boundary, for example due to the effects of the structure of or stresses within the grain boundary. These effects depend upon the rotation angle of the grain boundary, so at angles other than 45° there may be more or fewer strong junctions, with a corresponding improvement or degradation of reproducibility. Another way to improve the reproducibility of a grain-boundary junction is by increasing its width, thereby increasing the number of strong junctions.

V. CONCLUSIONS

A variety of experimental behaviors of $\Delta I_{dc}(I_{ac})$ for both integral and half-integral constant voltage steps in high-T_c grain-boundary junctions were classified. These behaviors were all reproduced by simulations of $\Delta i_{dc}(i_{ac})$ for two or three junctions in parallel. The excellent agreement between experimental and simulation results provides quantitative evidence that high-T_c grain-boundary junctions are composed of junctions in parallel. The complicated, nonperiodic behavior of $I_c(H)$ observed experimentally indicates that there are many junctions in parallel. A model of grain-boundary junctions based on superconducting filaments randomly distributed on either side of the grain boundary can explain all the experimental results. The overlap of two filaments on either side of the grain boundary forms a junction, whose critical current is proportional to the area of overlap. Due to the random distribution of filaments, only a few strong junctions are formed. Based on observations of half-integral steps in junctions with various widths, for 45° grain-boundary junctions these strong junctions are ~ 20 μm apart. The many junctions that are formed in this manner result in a complicated $I_c(H)$ behavior, while the few strong junctions determine the behavior of $\Delta I_{dc}(I_{ac})$ for both the integral and half-integral steps. There are

some indications, based on simulations of many (≥ 6) junctions in parallel, that some relative critical currents may be preferred when junctions are formed by the overlap of filaments. Further experiments and simulations should provide answers to this question, and thus give further information about the microstructural origin of junctions within high-T_c grain-boundary junctions.

ACKNOWLEDGMENTS

We thank C. J. Lobb and R. L. Kautz for useful discussions. This work was supported by the Electricity Division, National Institute of Standards and Technology, Technology Administration, U.S. Dept. of Commerce.

[1]P. Chaudhari, J. Mannhart, D. Dimos, C. C. Tsuei, J. Chi, M. M. Oprysko, and M. Scheuermann, Phys. Rev. Lett. **60**, 1653 (1988).

[2]S. E. Russek, D. K. Lathrop, B. H. Moeckly, R. A. Buhrman, D. H. Shin, and J. Silcox, Appl. Phys. Lett. **57**, 1155 (1990).

[3]K. Char, M. S. Colclough, L. P. Lee, and G. Zaharchuk, Physica C **185-189**, 2561 (1991).

[4]D. Dimos, P. Chaudhari, and J. Mannhart, Phys. Rev. B **41**, 4038 (1990).

[5]R. Gross, P. Chaudhari, M. Kawasaki, and A. Gupta, IEEE Trans. Magn. **MAG-27**, 3227 (1991).

[6]D. K. Lathrop, B. H. Moeckly, S. E. Russek, and R. A. Buhrman, Appl. Phys. Lett. **58**, 1095 (1991).

[7]D. C. Larbalestier, S. E. Babcock, X. Cai, L. Cooley, M. Däumling, D. P. Hampshire, J. McKinnell, and J. Seuntjens, *Progress in High-Temperature Superconductivity,* Proceedings of the Tokai University International Workshop on the Science of Superconductivity and New Materials, edited by S. Nakajima (World Scientific, New Jersey, 1989), Vol. 18, p. 128.

[8]M. Däumling, E. Sarnelli, P. Chaudhari, A. Gupta, and J. Lacey, Appl. Phys. Lett. **61**, 1355 (1992).

[9]E. Sarnelli, P. Chaudhari, and J. Lacey, Appl. Phys. Lett. **62**, 777 (1993).

[10]M. Kawasaki, P. Chaudhari, and A. Gupta, Phys. Rev. Lett. **68**, 1065 (1992).

[11]A. H. Miklich, J. Clarke, M. S. Colclough, and K. Char, Appl. Phys. Lett. **60**, 1899 (1992).

[12]B. H. Moeckly, D. K. Lathrop, and R. A. Buhrman, Phys. Rev. B **47**, 400 (1993).

[13]E. A. Early, A. F. Clark, and K. Char, Appl. Phys. Lett. **62**, 3357 (1993).

[14]B. D. Josephson, Phys. Lett. **1**, 251 (1962).

[15]S. Shapiro, Phys. Rev. Lett. **11**, 80 (1963).

[16]K. Char, M. S. Colclough, S. M. Garrison, N. Newman, and G. Zaharchuk, Appl. Phys. Lett. **59**, 733 (1991).

[17]K. Char, M. S. Colclough, L. P. Lee, and G. Zaharchuk, Appl. Phys. Lett. **59**, 2177 (1991).

[18]W. C. Stewart, Appl. Phys. Lett. **12**, 277 (1968).

[19]D. E. McCumber, J. Appl. Phys. **39**, 3113 (1968).

[20]P. A. Rosenthal, M. R. Beasley, K. Char, M. S. Colclough, and G. Zaharchuk, Appl. Phys. Lett. **59**, 3482 (1991).

[21]P. Russer, J. Appl. Phys. **43**, 2008 (1972).

[22]D. B. Sullivan, R. L. Peterson, V. E. Kose, and J. E. Zimmerman, J. Appl. Phys. **41**, 4865 (1970).

[23]J. Clarke, Phys. Rev. Lett. **21**, 1566 (1968).

[24]C. A. Hamilton and E. G. Johnson, Jr., Phys. Lett. A **41**, 393 (1972).

[25]H. Lübbig and H. Luther, Rev. Phys. Appl. **9**, 29 (1974).

[26]K. H. Gundlach and J. Kadlec, J. Low Temp. Phys. **26**, 603 (1977).

[27]S. P. Benz, M. S. Rzchowski, M. Tinkham, and C. J. Lobb, Phys. Rev. Lett. **64**, 693 (1990).

[28]H. C. Lee, R. S. Newrock, D. B. Mast, S. E. Hebboul, J. C. Garland, and C. J. Lobb, Phys. Rev. B **44**, 921 (1991).

[29]T. A. Fulton, L. N. Dunkleberger, and R. C. Dynes, Phys. Rev. B **6**, 855 (1972).

[30]C. D. Tesche and J. Clarke, J. Low Temp. Phys. **29**, 301 (1977).

[31]C. Vanneste, C. C. Chi, W. J. Gallagher, A. W. Kleinsasser, S. I. Raider, and R. L. Sandstrom, J. Appl. Phys. **64**, 242 (1988).

[32]V. N. Belykh, N. F. Pedersen, and O. H. Soerensen, Phys. Rev. B **16**, 4860 (1977).

[33]R. L. Kautz, J. Appl. Phys. **52**, 3528 (1981).

[34]K. K. Likharev, *Dynamics of Josephson Junctions and Circuits* (Gordon and Breach, Philadelphia, 1986), p. 260.

[35]P. G. De Gennes, Rev. Mod. Phys. **36**, 225 (1964).

[36]B. Mayer, S. Schuster, A. Beck, L. Alff, and R. Gross, Appl. Phys. Lett. **62**, 783 (1993).

[37]M. B. Ketchen, W. J. Gallagher, A. W. Kleinsasser, S. Murphy, and J. R. Clem, in *SQUID '85,* edited by H. D. Hahlbohm and H. Lübbig (Walter de Gruyter, Berlin, 1985), p. 865.

[38]For a recent review, see S. E. Babcock, Mater. Res. Soc. Bull. **17**, 20 (1992).